Electronic Supplementary Material (ESI) for Nanoscale.
This journal is © The Royal Society of Chemistry 2017

Electronic Supplementary Information

Cobalt ions-coordinated self-assembly synthesis of nitrogen-doped ordered mesoporous carbon nanosheets for efficiently catalyzing oxygen reduction

Haitao Wang, Wei Wang, Muhammad Asif, Yang Yu, Zhengyun Wang, Junlei Wang, Hongfang Liu and Junwu Xiao**

Key Laboratory of Material Chemistry for Energy Conversion and Storage, Ministry of Education, Hubei Key Laboratory of Material Chemistry and Service Failure, School of Chemistry and Chemical Engineering, Huazhong University of Science and Technology, Wuhan, 430074, P. R. China.

*** Corresponding Author**

Tel: +8615872409866, E-mail: chjwxiao@hust.edu.cn (J. Xiao).

Tel: +8613638673026, E-mail: liuhf@hust.edu.cn (H. Liu).

Experimental section

1.1 Synthesis of Co/N-OMCNS

In a typical synthesis, triblock copolymer Pluronic F127 (2 g), 3-aminophenol (1 g), HMTA (0.80 g) and $Co(CH_3COO)_2 \cdot 4H_2O$ (0.25 g) are dissolve in 60 mL deionized water until form a homogeneous pink solution at room temperature, then 28 wt% aqueous ammonia (2 mL) is added to the above solution. Next, the result solution is poured into an airtight glass reactor and heated at 80 °C with constant stirring for 24 h to form Co containing nitrogen-rich carbon polymer nanosheet (Co/N-CPS). The as-made brown Co/N-CPS product is collected by centrifugation, washed three times with water, and desiccation at 60 °C overnight. Finally, the Co/N-CPS is pyrolyzed at different temperatures (T = 600, 700, 800 and 900 °C) under argon atmosphere with a ramp rate of 3 °C min^{-1} for 2 h. After that, Co/N-OMCNS-T are obtained. For comparison, Co-free sample N-CPS and N-OMCNS are synthesized by a similar method, apart from $Co(CH_3COO)_2 \cdot 4H_2O$ is used.

1.2 Physical characterization

The morphologies of the obtained samples are examined by scanning electron microscopy (SEM, Nova NanoSEM 450) operated at 10 kV. The microstructure is studied by transmission electron microscopy (TEM) using a Tecnai G2 20 microscope operating at 200 kV. Powder X-ray diffraction (XRD) is conducted on a Philips PW-1830 X-ray diffractometer at a rate of 5 °C $min^{-}1$. Raman analysis are carried out using a LabRAM HR800 confocal Raman microscope. X-ray photoelectron spectroscopy (XPS) data is recorded on an AXIS-ULTRA DLD-600W instrument. The N_2 adsorption/desorption isotherms are collected using a Micromeritics ASAP

2020 instruments at 77 K.

1.3 Electrochemical measurements

All the electrochemical tests are evaluated on a conventional three-electrode cell by a CHI 760E electrochemical workstation (CH Instruments, China) with the Pine rotating ring disk electrode system (a Pine biopotentiostat and a rotation speed controller) at 25°C. A saturated calomel electrode (SCE) and a platinum foil are used as the reference electrode and counter electrode. In particular, the used SCE electrode is protected with salt bridge, which can effectively avoid the penetration of alkaline medium into the SCE electrode. The working electrode is prepared as follows: 5 mg of the sample is ultrasonically dispersed in 1 mL Nafion/ethanol solution (contained 0.02 mL of 5 wt% nafion solution) for at least 30 min, then 14 μL of the homogeneous dispersion is pipetted onto the glassy carbon electrode (5 mm inner diameter) surface, drying under infrared illumination. For comparison, the loading quantity of commercial Pt/C (20%, E-TEK) is 0.102 mg cm^{-2}. All potentials in this paper are calibrated with respect to RHE ($E_{(RHE)} = E_{(SCE)} + 0.059 \bullet pH + 0.242$ V). Before electrochemical tests, the N_2 or O_2 flow is used to achieve the N_2 or O_2-saturated 0.1 M KOH electrolyte. Cyclic voltammogram (CV) curves are collected at a scan rate of 50 mV s^{-1} from 0.0 V to 1.2 V (vs. RHE) in N_2 or O_2-saturated 0.1 M KOH solution. Linear sweep voltammetry (LSV) measurements are performed in N_2 or O_2-saturated 0.1 M KOH solution with a scan rate of 5 mV s^{-1} at the different rotation rates (625 rpm-2500 rpm). Koutecky-Levich plots (K-L plots) at various electrode potentials are analyzed to calculate the kinetic current density (J_K) and number of electrons transferred (n) for the ORR on the strength of K-L equation as below:

$$J^{-1} = J_L^{-1} + J_K^{-1} = B^{-1}\omega^{-1/2} + J_K^{-1} \quad (1)$$

$$B = 0.2nFC_0D_0^{2/3}\upsilon^{-1/6} \quad (2)$$

$$J_K = nFkC_0 \quad (3)$$

Where J and J_L are the measured current density and diffusion limiting currents density, respectively, ω is the rotation speed (rpm), F is the Faraday constant (F = 96 485 C mol^{-1}), C_0 is the bulk concentration of O_2 ($C_0 = 1.21 \cdot 10^{-6}$ mol L^{-1}), D_0 is the O_2 diffusion coefficient ($D_0 = 1.9 \cdot 10^{-5}$ cm^2 s^{-1}), υ is the kinematic viscosity of the electrolyte ($\upsilon = 0.01$ cm^2 s^{-1}) and k is the electron-transfer rate constant.

For methanol poisoning measurements, the chronoamperometric response at 0.6V is recorded at the rotation rate of 1600 rpm in O_2-saturated 0.1 M KOH solution with 2 M methanol. The durability testing of samples and commercial Pt/C are conducted by continuous potential cycling from 0.0 V to 1.2 V (vs. RHE) in O_2-saturated 0.1 M KOH electrolyte with a scan rate of 100 mV s^{-1}. The stability testing is also recorded using the chronoamperometric technique at 0.6 V in O_2-saturated 0.1 M KOH solution with the rotation rate of 1600 rpm for 50000 s.

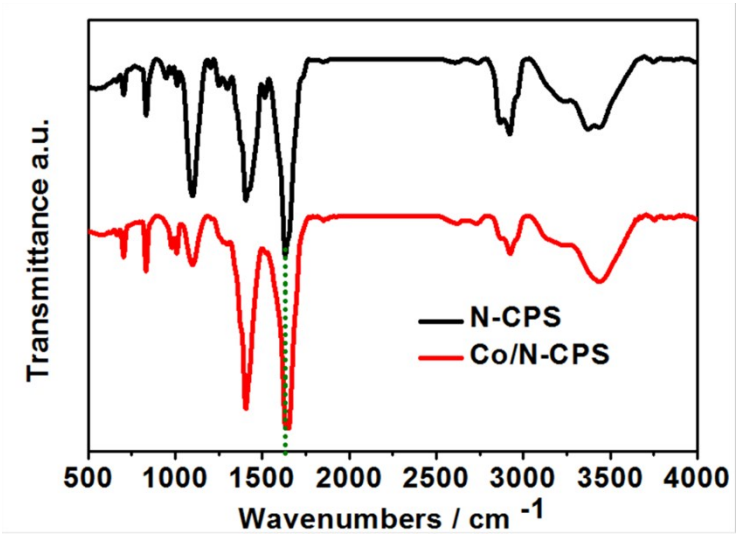

Figure S1. FTIR spectra of N-CPS and Co/N-CPS.

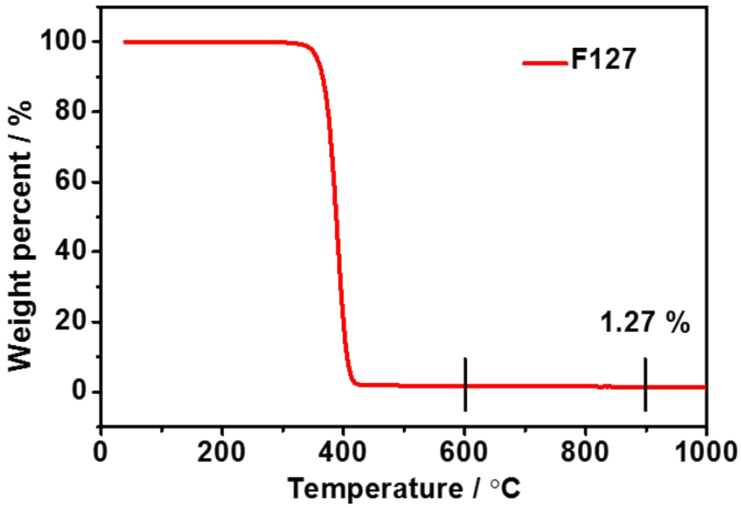

Figure S2. Thermogravimetric analysis (TGA) of F127 block copolymer under argon flow.

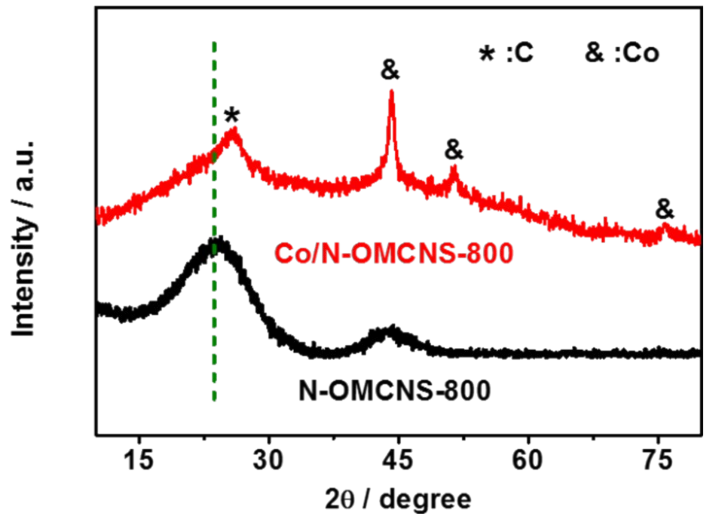

Figure S3. XRD patterns of N-OMCNS-800 and Co/N-OMCNS-800.

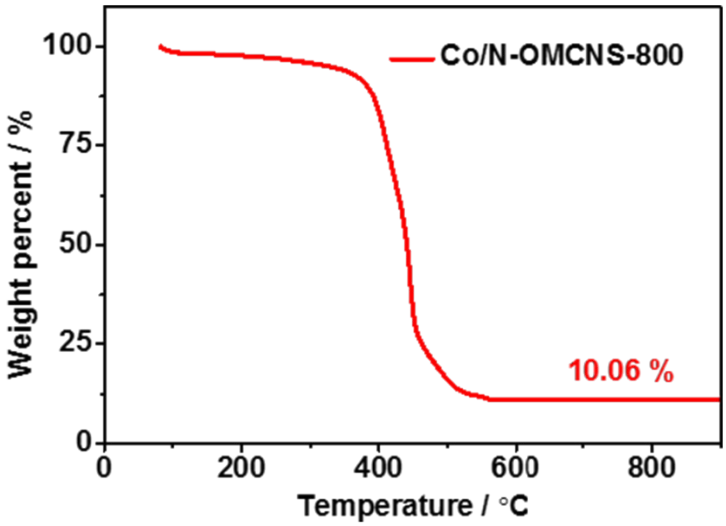

Figure S4. Thermogravimetric analysis (TGA) under air flow. The solid product after TGA corresponds to Co_3O_4, thus the weight percent of Co is about 7.39 wt%.

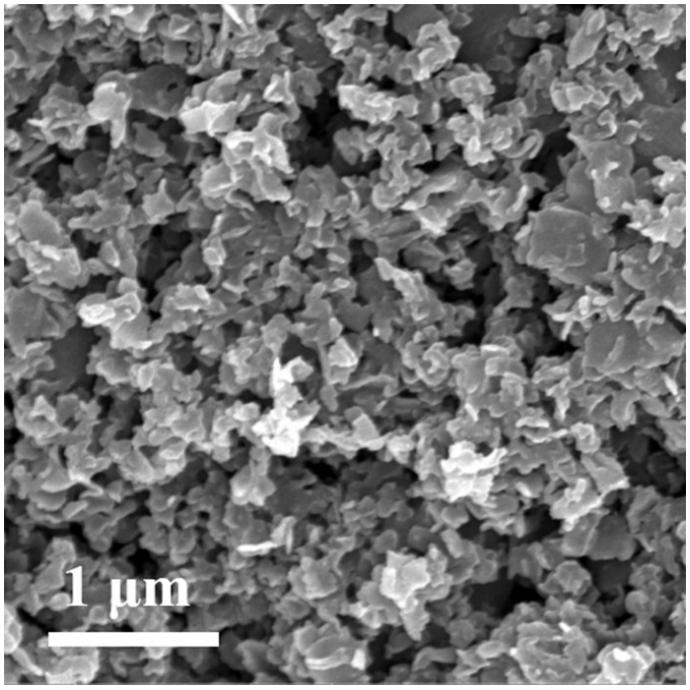

Figure S5. FESEM image of Co/N-OMCNS-800 obtained using a large amount of $Co(CH_3COO)_2 \cdot 4H_2O$ (0.40 g) in the process of synthesis.

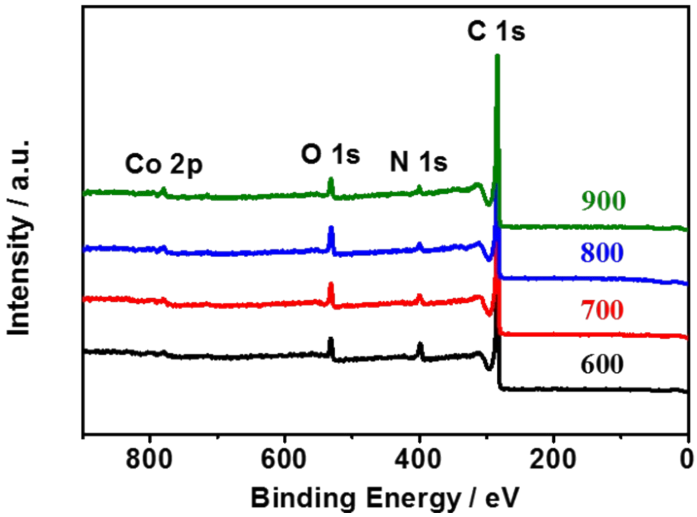

Figure S6. XPS survey spectra of Co/N-OMCNS.

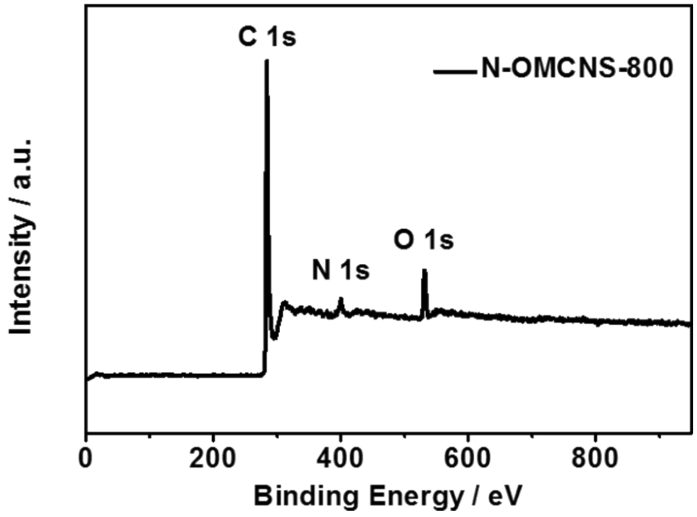

Figure S7. XPS survey spectra of N-OMCNS-800.

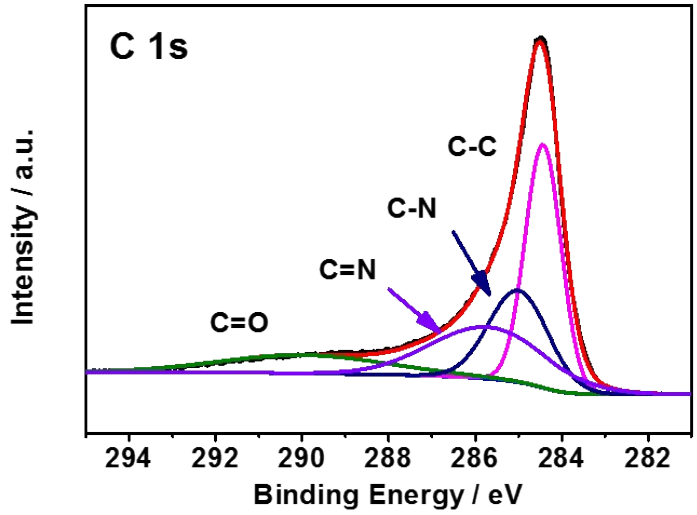

Figure S8. High resolution C 1s XPS survey spectra of Co/N-OMCNS-800.

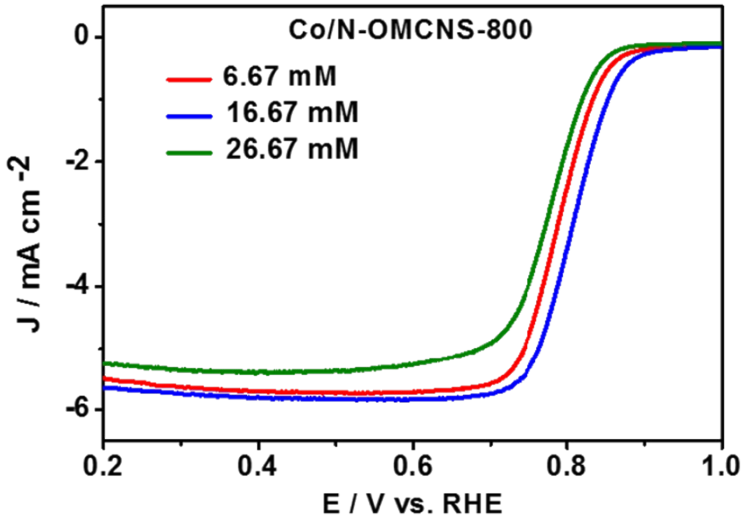

Figure S9. LSV curves of Co/N-OMCNS-800 formed at the different concentrations of Co^{2+} during the preparation.

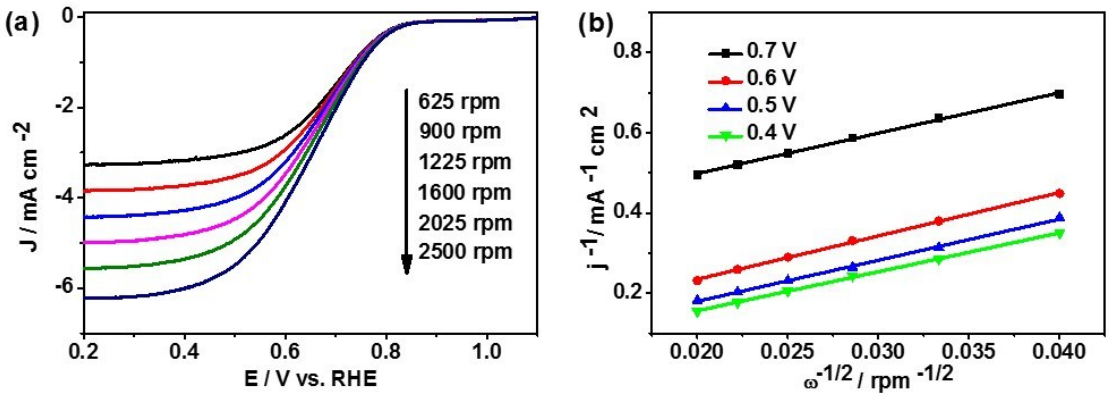

Figure S10. (a) LSVs at different rotation rates of Co/N-OMCNS-600 and (b) the corresponding K-L plots at the potential range of 0.4 V to 0.7 V.

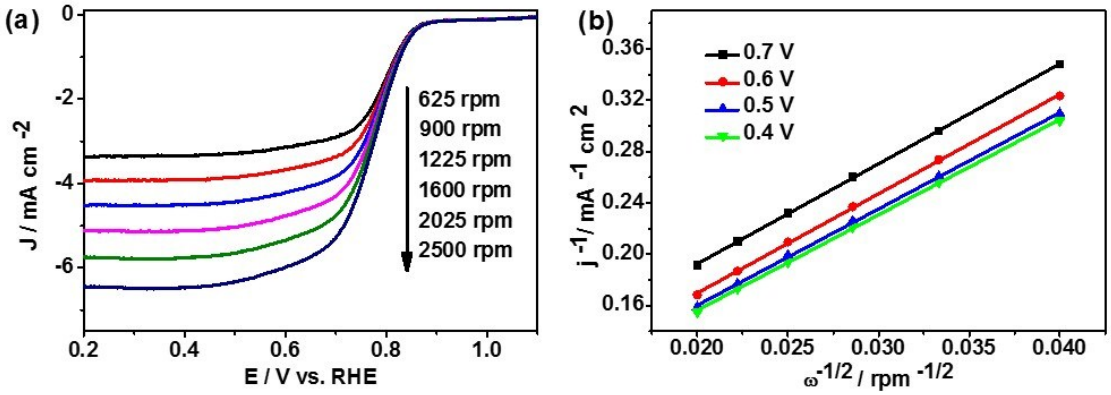

Figure S11. (a) LSVs at different rotation rates of Co/N-OMCNS-700 and (b) the corresponding K-L plots at the potential range of 0.4 V to 0.7 V.

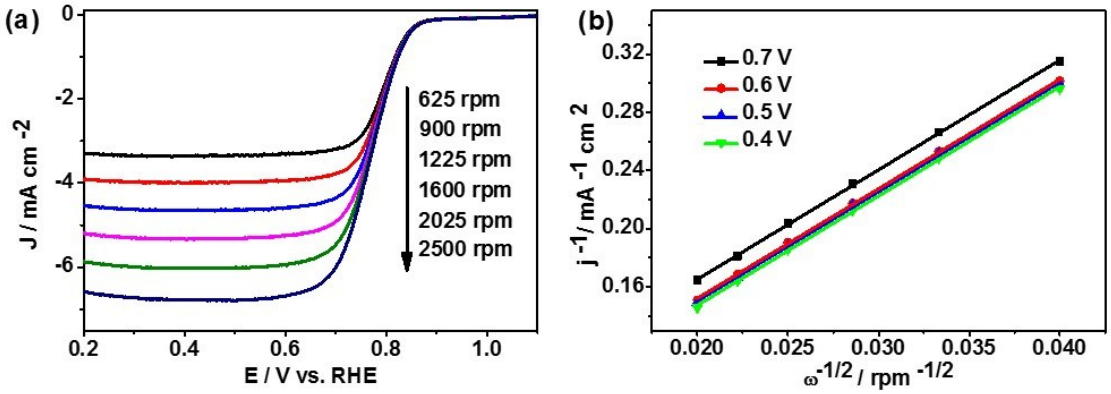

Figure S12. (a) LSVs at different rotation rates of Co/N-OMCNS-900 and (b) the corresponding K-L plots at the potential range of 0.4 V to 0.7 V.

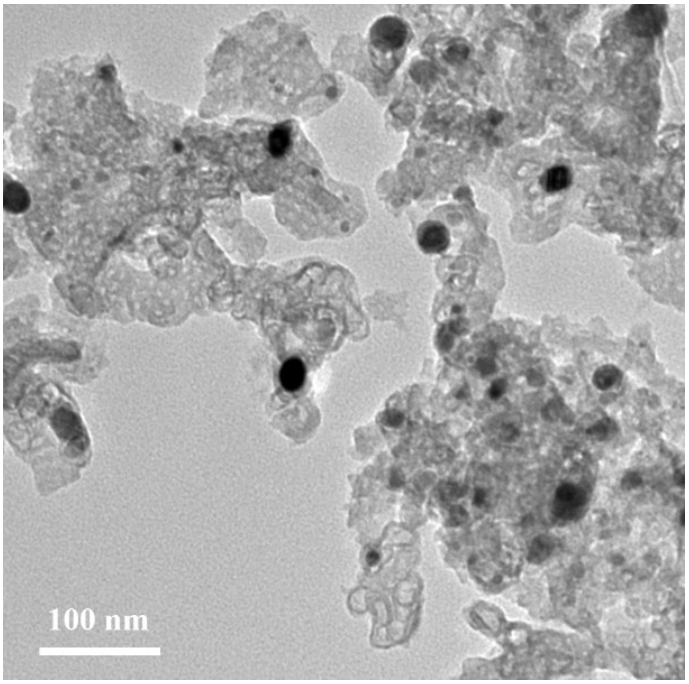

Figure S13. TEM image of Co/N-OMCNS-900

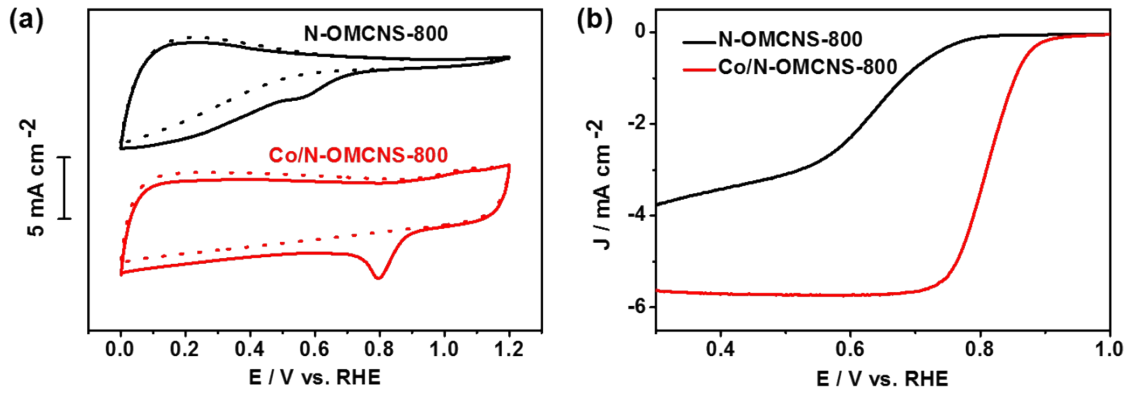

Figure S14. (a) CVs of N-OMCNS-800 and Co/N-OMCNS-800 in N_2 or O_2-saturated 0.1 M KOH. (b) LSVs of N-OMCNS-800 and Co/N-OMCNS-800.

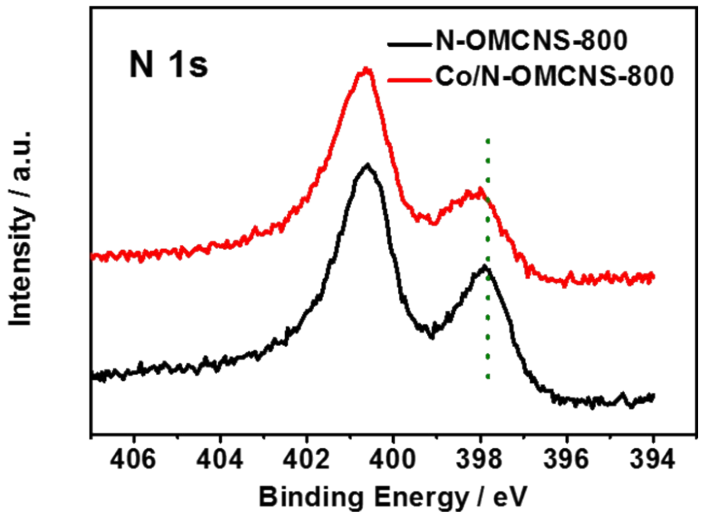

Figure S15. High resolution N 1s spectrum of N-OMCNS-800 and Co/N-OMCNS-800.

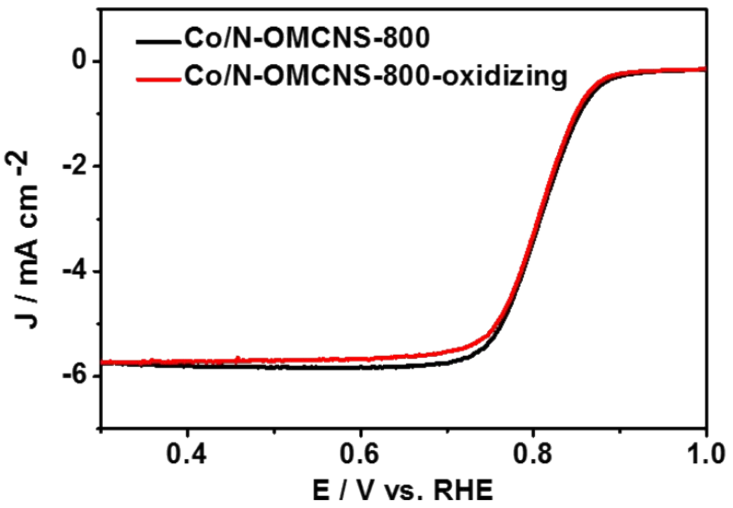

Figure S16. LSVs of Co/N-OMCNS-800 and Co/N-OMCNS-800-oxidizing in O2-saturated 0.1 M KOH.

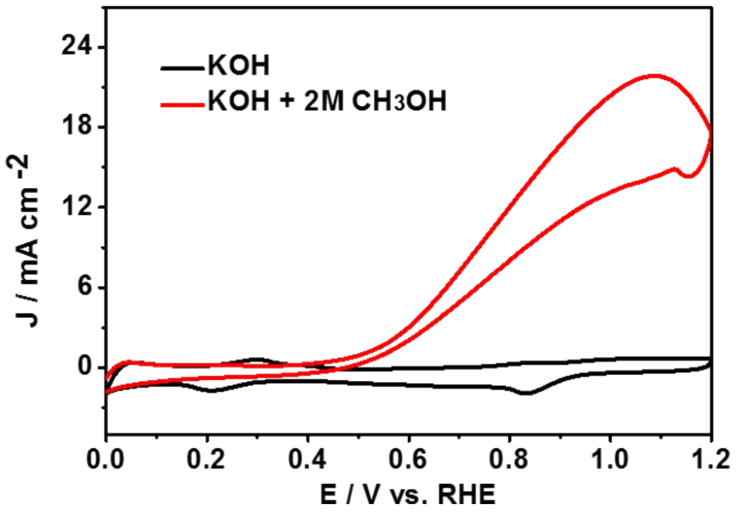

Figure S17. CVs of 20% Pt/C in O_2-staturated (black) or in the presence of 2 M methanol O_2-staturated (red) 0.1 M KOH.

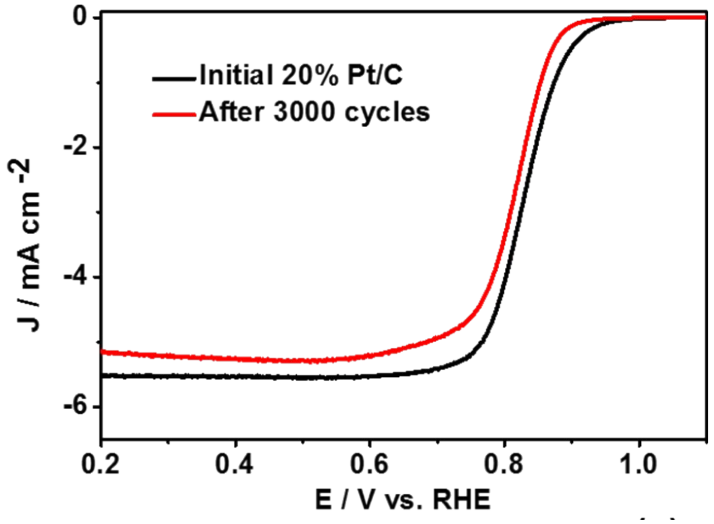

Figure S18. LSVs of 20% Pt/C before and after 3000 potential cycles at the potential range of 0 V to 1.2 V in O_2-saturated 0.1 M KOH.

Table S1. BET surface area, total pore volume and average pore size of Co/N-OMCNS.

Sample	BET surface area (m^2 g^{-1})	Total pore volume (cm^3 g^{-1})	Average pore size (nm)
Co/N-OMCNS-600	605.8	0.61	3.49
Co/N-OMCNS-700	565.4	0.52	3.86
Co/N-OMCNS-800	536.9	0.50	4.11
Co/N-OMCNS-900	456.1	0.45	5.86

Table S2. The content of C, N, O and Co for Co/N-OMCNS.

Sample	C (at %)	N (at %)	O (at %)	Co (at %)
Co/N-OMCNS-600	90.46	5.05	4.28	0.21
Co/N-OMCNS-700	92.09	3.76	3.87	0.28
Co/N-OMCNS-800	92.64	2.75	4.18	0.43
Co/N-OMCNS-900	93.35	1.77	4.36	0.52

Table S3. The content of Co and N for Co/N-OMCNS obtained using different pyrolysis temperatures and the fractions of the different N species measured by XPS (The brackets contained the absolute contents of the different N species).

Sample	Co (at %)	N (at %)	Graphitic N % (at %)	Pyrrolic N % (at %)	Pyridinic N % (at %)
Co/N-OMCNS-600	0.21	5.05	9.87 (0.50)	46.65 (2.36)	43.48 (2.19)
Co/N-OMCNS-700	0.28	3.76	19.62 (0.74)	43.82 (1.65)	36.56 (1.37)
Co/N-OMCNS-800	0.43	2.75	33.71 (0.93)	40.42 (1.11)	25.87 (0.71)
Co/N-OMCNS-900	0.52	1.77	49.37 (0.87)	35.28 (0.62)	15.35 (0.28)

Table S4. The comparison of the E_P, E_0, $E_{1/2}$ and J_i for ORR of Co/N-OMCNS in O_2 saturated 0.1 M KOH at the rotation of 1600 rpm.

Sample	E_p vs RHE (V)	E_0 vs RHE (V)	$E_{1/2}$ vs RHE (V)	J_i vs RHE (mA cm^{-2})
Co/N-OMCNS-600	0.657	0.876	0.672	4.92
Co/N-OMCNS-700	0.766	0.942	0.783	5.16
Co/N-OMCNS-800	0.804	0.961	0.815	5.64
Co/N-OMCNS-900	0.751	0.921	0.772	5.37
20% Pt/C	0.828	0.996	0.832	5.54

E_0: defined as the corresponding potential when ORR current density reaches 0.1 mA cm^{-2}.

J_i: defined as the corresponding current density at the potential of 0.3 V.

Table S5 Comparison of the ORR electrochemical activity in terms of E_P, E_0 and $E_{1/2}$ among the Co based related catalysts in 0.1 M KOH reported so far.

Catalysts	Loading (mg cm^{-2})	E_p vs RHE (V)	E_0 vs RHE (V)	$E_{1/2}$ vs RHE (V)	References
Co/N-OMCNS-800	**0.357**	**0.804**	**0.961**	**0.815**	**This work**
Co@CoO@N–C/C	0.421	0.790	0.920	0.810	1
CoP-CMP800	0.600	0.790	0.890	0.815	2
Co@Co_3O_4@C-CM	0.100	0.790	0.930	0.810	3
YS-Co/N-PCMs	0.272	0.776	0.922	0.788	4
SUCo-0.1-800	—	0.780	0.945	0.793	5
Co/N-C-800	0.250	0.733	0.834	0.730	6
N–C@Co-2	0.213	0.800	0.895	0.805	7
Co_2FeO_4/MWCNT	0.397	0.700	0.910	0.730	8
CoO@N/S-CNF	0.080	0.740	0.840	0.760	9
Co/N-HCOs	0.272	0.790	0.920	0.810	10
Co_2C/GO	0.256	0.802	0.919	0.814	11
CoO/rGO (N)	0.256	—	0.940	0.810	12
Co-C@NWCs	0.100	—	0.939	0.820	13
Co_3O_4/N-rmGO	0.100	0.830	0.930	0.830	14
CoOx/Co@GC-NC	0.464	0.835	0.974	0.858	15
CoSAs/NC(800)	0.408	—	0.959	0.863	16

Supplementary References

[1] Wu, Z.; Wang, J.; Han, L.; Lin, R.; Liu, H.; Xin, H. L.; Wang, D., Supramolecular Gel-Assisted Synthesis of Double Shelled Co@CoO@N–C/C Nanoparticles with Synergistic Electrocatalytic Activity for the Oxygen Reduction Reaction. *Nanoscale* **2016**, *8,* 4681-4687.

[2] Wu, Z. S.; Chen, L.; Liu, J.; Parvez, K.; Liang, H.; Shu, J.; Sachdev, H.; Graf, R.; Feng, X.; Müllen, K., High-Performance Electrocatalysts for Oxygen Reduction Derived from Cobalt Porphyrin-Based Conjugated Mesoporous Polymers. *Adv. Mater.* **2014**, *26,* 1450-1455.

[3] Xia, W.; Zou, R.; An, L.; Xia, D.; Guo, S., A Metal-Organic Framework Route to in Situ Encapsulation of Co@Co_3O_4@C Core@Bishell Nanoparticles into a Highly Ordered Porous Carbon Matrix for Oxygen Reduction. *Energy Environ. Sci.* **2015**, *8,* 568-576.

[4] Chao, S.; Cui, Q.; Wang, K.; Bai, Z.; Yang, L.; Qiao, J., Template-Free Synthesis of Hierarchical Yolk-Shell Co and N Codoped Porous Carbon Microspheres With Enhanced Performance for Oxygen Reduction Reaction. *J. Power Sources* **2015**, *288,* 128-135.

[5] Zhang, G.; Lu, W.; Cao, F.; Xiao, Z.; Zheng, X., N-doped Graphene Coupled with Co Nanoparticles as an Efficient Electrocatalyst for Oxygen Reduction in Alkaline Media. *J. Power Sources* **2016**, *302*, 114-125.

[6] Su, Y.; Zhu, Y.; Jiang, H.; Shen, J.; Yang, X.; Zou, W.; Chen, J.; Li, C., Cobalt Nanoparticles Embedded in N-doped Carbon as an Efficient Bifunctional Electrocatalyst for Oxygen Reduction and Evolution Reactions. *Nanoscale* **2014**, *6,* 15080-15089.

[7] Han, C.; Bo, X.; Zhang, Y.; Li, M.; Nsabimana, A.; Guo, L., N-doped Graphitic Layer Encased Cobalt Nanoparticles as Efficient Oxygen Reduction Catalysts in Alkaline Media. *Nanoscale* **2015**, *7,* 5607-5611.

[8] Wang, J.; Xin, H. L.; Zhu, J.; Liu, S.; Wu, Z.; Wang, D., 3D Hollow Structured Co_2FeO_4/MWCNT as an Efficient Non-Precious Metal Electrocatalyst for Oxygen Reduction Reaction. *J. Mater. Chem. A* **2015**, *3,* 1601-1608.

[9] Liu, T.; Guo, Y.-F.; Yan, Y.-M.; Wang, F.; Deng, C.; Rooney, D.; Sun, K.-N., CoO Nanoparticles Embedded in Three-Dimensional Nitrogen/Sulfur Co-Doped Carbon Nanofiber Networks as a Bifunctional Catalyst for Oxygen Reduction/Evolution Reactions. *Carbon* **2016,** *106,* 84-92.

[10] Chao, S.; Bai, Z.; Cui, Q.; Yan, H.; Wang, K.; Yang, L., Hollowed-Out Octahedral Co/N-Codoped Carbon as a Highly Efficient Non-Precious Metal Catalyst for Oxygen Reduction Reaction. *Carbon* **2015**, *82,* 77-86.

[11] Meganathan, M. D.; Mao, S.; Huang, T.; Sun, G., Reduced graphene oxide intercalated Co_2C or Co_4N nanoparticles as an efficient and durable fuel cell catalyst for oxygen reduction. *J. Mater. Chem. A* **2017**, *5*, 2972-2980.

[12] He, Q.; Li, Q.; Khene, S.; Ren, X.; López-Suárez, F. E.; Lozano-Castelló, D.; Bueno-López, A.; Wu, G., High-loading cobalt oxide coupled with nitrogen-doped graphene for oxygen reduction in anion-exchange-membrane alkaline fuel cells. *J. Phys. Chem. C* **2013**, *117*, 8697-8707.

[13] Li, Y.; Cheng, F.; Zhang, J.; Chen, Z.; Xu, Q.; Guo, S., Cobalt-Carbon Core-Shell Nanoparticles Aligned on Wrinkle of N‐Doped Carbon Nanosheets with Pt-Like Activity for Oxygen Reduction. *Small* **2016**, *12*, 2839-2845.

[14] Liang, Y.; Li, Y.; Wang, H.; Zhou, J.; Wang, J.; Regier, T.; Dai, H., Co_3O_4 nanocrystals on graphene as a synergistic catalyst for oxygen reduction reaction. *Nat. Mater.* **2011**, *10*, 780-786.

[15] Yu, J.; Chen, G.; Sunarso, J.; Zhu, Y.; Ran, R.; Zhu, Z.; Zhou, W.; Shao, Z., Cobalt Oxide and Cobalt-Graphitic Carbon Core-Shell Based Catalysts with Remarkably High Oxygen Reduction Reaction Activity. *Adv. Sci*. **2016**, *3*, 1600060.

[16] Yin, P.; Yao, T.; Wu, Y.; Zheng, L.; Lin, Y.; Liu, W.; Ju, H.; Zhu, J.; Hong, X.; Deng, Z., Single Cobalt Atoms with Precise N-Coordination as Superior Oxygen Reduction Reaction Catalysts. *Angew. Chem. Int. Ed.* **2016**, *55*, 10800-10805.